Order reconstruction in frustrated nematic twist cells

Fulvio Bisi,[1,*] Eugene C. Gartland, Jr.,[2] Riccardo Rosso,[1] and Epifanio G. Virga[1]
[1]*Dipartimento di Matematica, Istituto Nazionale di Fisica della Materia, Università di Pavia, via Ferrata 1, 27100 Pavia, Italy*
[2]*Department of Mathematical Sciences, Kent State University, Kent, Ohio 44242, USA*
(Received 20 May 2003; published 27 August 2003)

Within the Landau–de Gennes theory of liquid crystals, we study the equilibrium configurations of a nematic cell with twist boundary conditions. Under the assumption that the order tensor **Q** be uniaxial on both bounding plates, we find three separate classes of solutions, one of which contains the absolute energy minimizer, a *twistlike* solution that exists for all values of the distance d between the plates. The solutions in the remaining two classes exist only if d exceeds a critical value d_c. One class consists of metastable, twistlike solutions, while the other consists of unstable, *exchangelike* solutions, where the eigenvalues of **Q** are exchanged across the cell. When $d=d_c$, the metastable solution relaxes back to the absolute energy minimizer, undergoing an order reconstruction somewhere within the cell. The critical distance d_c equals, in general, a few biaxial coherence lengths. This scenario applies to all the values of the boundary twist but $\pi/2$, which thus appears as a very special case, though it is the one more studied in the literature. In fact, when the directors prescribed on the two plates are at right angles, two symmetric twistlike solutions merge continuously into an exchangelike solution at the critical value of d where the latter becomes unstable. Our analysis shows how the classical bifurcation associated with this phenomenon is *unfolded* by perturbing the boundary conditions.

DOI: 10.1103/PhysRevE.68.021707 PACS number(s): 61.30.Gd, 61.30.Pq

I. INTRODUCTION

Defects and microconfinements in liquid crystals are both very interesting subjects, still offering unsolved problems. Different as they may appear, these subjects have a common feature, that is, material *frustration*. In the absence of external fields, frustration in nematic liquid crystals is ultimately produced by the bounding surfaces: indirectly when they dictate the presence of defects in the bulk, and directly when they cause extreme confinements of the material. Both defects and microconfinements bear on *order reconstruction*. For defects, this was first shown by Schopohl and Sluckin in Ref. [1], who found that within the core of a disclination, two uniaxial states with orthogonal directors are changed into each other through a transformation that does not involve any director rotation, but instead implies a wealth of biaxial configurations bridging the uniaxial limits. Likewise, in a hybrid cell, which here serves as a paradigm of all confined nematic systems, Palffy-Muhoray, Gartland, and Kelly [2] showed that the two orthogonal uniaxial directors prescribed on the plates (one planar and the other homeotropic) can be connected either through a director bend or through an order reconstruction which employs biaxial states. An interesting result of Ref. [2] is that when the cell thickness is sufficiently small, only the order reconstruction exists as an equilibrium configuration for the free energy of the cell.

In the terminology used in both Refs. [1,2], this surviving solution exhibits an *eigenvalue exchange*: in the tensorial description of the nematic order, two uniaxial states with orthogonal directors can indeed be connected with no eigenframe rotation by only changing the eigenvector that possesses the dominant eigenvalue. This conclusion was reached under the assumption that the anchoring be strong on both bounding plates. For weak anchorings, a similar lack of solution had been already obtained in Ref. [3], but only within the classical director theory: when the distance between the plates becomes smaller than a critical value, the bent director configuration ceases to be an equilibrium solution, and the energy minimizer is the uniform field with the least anchoring energy. Many studies further built on the outcomes of Ref. [2]. First, in Ref. [4] the analysis was extended to cover also weak anchoring conditions. More recently, the fluctuations of both the eigenvalues and the eigenframe of the order tensor have been studied for the ground state of a hybrid cell to compute the Casimir forces in distorted, frustrated configurations [5–7].

In all these studies, however, the easy axes of the plates are invariably at right angles. Our analysis starts from relaxing this condition. The scenario we thus unveil could be significant also for more general confinements. We consider a twist cell with strong anchoring on the two plates. The boundary states are prescribed to be uniaxial, while the internal states can possibly be biaxial. If the easy axes on the plates fail to be orthogonal, then there are two equilibrium twisted configurations, one more strained than the other. These configurations are both locally stable. Upon decreasing the distance between the plates, the less strained configuration persists as an equilibrium solution, whereas the more strained configuration ceases to exist at a critical value of the cell thickness. The ''exchange'' solution, which also only exists above this critical thickness, is locally unstable and merges in with the more strained solution just when this latter disappears.

We shall see how the symmetric ''pitchfork'' bifurcation diagram associated with the $\pi/2$-twist configuration transforms into a perturbed diagram, with two disconnected branches, upon breaking the clockwise-counterclockwise symmetry in the boundary conditions with orthogonal direc-

*Electronic address: bisi@dimat.unipv.it;
URL: http://smmm.unipv.it

tors, a process often called *bifurcation unfolding*. We conclude that in the broken-symmetry case, if the alignment within the cell were initially trapped into the metastable, more strained configuration, then upon reducing the cell thickness, it would be forced to fall onto the stable, less strained configuration, where it would stay even once the thickness is increased above the critical value. It is remarkable that this structural transition still happens through an order reconstruction, which is necessarily dynamical, as it is accompanied by a discontinuity in the free energy.

The plan of the paper is as follows. In Sec. II, we present the mathematical model that describes a nematic twist cell. In Sec. III, we study the energetics of the model and write the equations that govern the equilibrium configurations. These are then solved numerically in Sec. IV in a variety of cases. Section V is devoted to illustrating the unfolding and perturbation of the bifurcation diagram: a limit point, instead of a bifurcation, illuminates the scenario outlined above. In Sec. VI, we discuss the relevance of boundary conditions to our outcomes, and the validity in our context of an approximation sometimes employed in the literature. Our conclusions are then summarized in Sec. VII.

II. MODEL

Most nematic liquid crystals can be thought of as composed of rodlike molecules. A nematic state can be described by the order tensor $\mathbf{Q}$, a symmetric, traceless, second-rank tensor that measures how much the probability distribution of the molecular long axis differs from being isotropic (see pp. 56–57 of Ref. [8]). Since $\mathbf{Q}$ is a symmetric tensor, it can be represented in the orthonormal basis of its eigenvectors $\{\boldsymbol{e}_1,\boldsymbol{e}_2,\boldsymbol{e}_3\}$ as

$$\mathbf{Q}=\sum_{i=1}^{3}\lambda_i\boldsymbol{e}_i\otimes\boldsymbol{e}_i,$$

where the eigenvalues λ_i obey the constraint

$$\lambda_1+\lambda_2+\lambda_3=0$$

implied by the condition $\mathrm{tr}\,\mathbf{Q}=0$. Moreover, each eigenvalue λ_i ranges in the interval $[-\frac{1}{3},\frac{2}{3}]$ (see pp. 14–18 of Ref. [9]): the lower bound corresponds to the case where the molecules are on average orthogonal to $\boldsymbol{e}_i$, whereas the upper bound corresponds to the case where the molecules are on average aligned along $\boldsymbol{e}_i$. In the isotropic phase, $\mathbf{Q}$ vanishes. When two eigenvalues of $\mathbf{Q}$ coincide, the liquid crystal is in a uniaxial state, and $\mathbf{Q}$ can be recast in the form

$$\mathbf{Q}=s\left(\boldsymbol{n}\otimes\boldsymbol{n}-\frac{1}{3}\mathbf{I}\right),$$

where $s\in[-\frac{1}{2},1]$ is the *scalar* order parameter, the unit vector $\boldsymbol{n}$ is the nematic *director*, and $\mathbf{I}$ is the identity tensor. Finally, when all eigenvalues of $\mathbf{Q}$ are distinct, the liquid crystal is in a biaxial state. According to Ref. [10], the *degree of biaxiality* of $\mathbf{Q}$ can be defined as

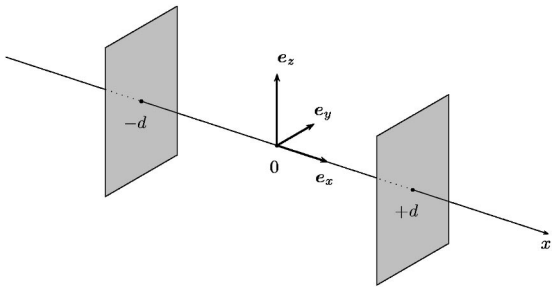

FIG. 1. A cell bounded by two parallel plates.

$$\beta^2:=1-6\frac{(\mathrm{tr}\,\mathbf{Q}^3)^2}{(\mathrm{tr}\,\mathbf{Q}^2)^3},\tag{1}$$

which ranges in the interval $[0,1]$. In all uniaxial states, $\beta^2=0$, while states with maximal biaxiality correspond to $\beta^2=1$. Since $\mathrm{tr}\,\mathbf{Q}^3=3\det\mathbf{Q}$, the states with maximal biaxiality are precisely those where $\det\mathbf{Q}=0$, that is, where at least one eigenvalue of $\mathbf{Q}$ vanishes.

We suppose that a nematic liquid crystal occupies the region $\mathcal{B}$ bounded by two parallel plates $2d$ apart (see Fig. 1). Relative to the frame $\{\boldsymbol{e}_x,\boldsymbol{e}_y,\boldsymbol{e}_z\}$ shown in Fig. 1, $\mathcal{B}$ is represented as the set $\mathcal{B}=\{(x,y,z)\in\mathbb{R}^3|x\in[-d,d]\}$. We impose uniaxial states at both plates. On the plate at $x=-d$, the nematic director is parallel to $\boldsymbol{e}_z$, so that

$$\mathbf{Q}=\mathbf{Q}^-:=s_b\left(\boldsymbol{e}_z\otimes\boldsymbol{e}_z-\frac{1}{3}\mathbf{I}\right),\tag{2}$$

where s_b is a *fixed* scalar order parameter, which we will set equal to the bulk equilibrium value for s. On the plate at $x=d$, the nematic director is rotated by the angle ϕ_0 (normalized to be in $[0,\pi/2]$), so that

$$\mathbf{Q}=\mathbf{Q}^+:=s_b\left(\boldsymbol{n}_0\otimes\boldsymbol{n}_0-\frac{1}{3}\mathbf{I}\right)\ \text{with}\ \boldsymbol{n}_0:=\cos\phi_0\boldsymbol{e}_z+\sin\phi_0\boldsymbol{e}_y.\tag{3}$$

In a purely uniaxial setting, the nematic director would twist within the cell from the orientation $\boldsymbol{e}_z$ to $\boldsymbol{n}_0$ as x ranges from $-d$ to d. In general, there are two opposite such twists, with one more strained than the other. They are mirror images of each other only for $\phi_0=\pi/2$, that is, when the boundary orientations of $\boldsymbol{n}$ are orthogonal. It is indeed the purpose of this paper to find the biaxial structure developed by both of these configurations and to seek other biaxial equilibrium configurations reminiscent of the one first discovered in Ref. [1] within a defect core, where two eigenvalues of $\mathbf{Q}$ cross each other and are eventually exchanged.

In general, $\mathbf{Q}$ is described by five independent scalar parameters. Here we exploit the particular symmetry of the problem to reduce the number of parameters. The boundary values $\mathbf{Q}^-$ and $\mathbf{Q}^+$ are indeed independent of the coordinates y and z, and they both have $\boldsymbol{e}_x$ as an eigenvector. By requiring these properties to hold for $\mathbf{Q}$ inside the cell, we arrive at the representation formula (in terms of Cartesian components)

$$[\mathbf{Q}]=\begin{bmatrix} -2q_1 & 0 & 0 \\ 0 & q_1-q_2 & q_3 \\ 0 & q_3 & q_1+q_2 \end{bmatrix}, \tag{4}$$

where q_1, q_2, and q_3 are functions of x only. This representation automatically obeys the constraint tr $\mathbf{Q}=0$. Hereafter, we shall refer to Eq. (4) as the *q representation* of $\mathbf{Q}$. The parameter q_3 measures the rotation around the $\boldsymbol{e}_x$ axis of the eigenframe of $\mathbf{Q}$. The eigenvalue relative to $\boldsymbol{e}_x$ is $\lambda_1=-2q_1$, while the remaining eigenvalues are

$$\lambda_2=q_1-\sqrt{q_2^2+q_3^2},\quad \lambda_3=q_1+\sqrt{q_2^2+q_3^2}.$$

We often employ the notation $q=(q_1,q_2,q_3)$ to denote a point in the q space. It follows from the bounds on the eigenvalues of $\mathbf{Q}$ that all admissible q's lie inside the cone with axis along q_1 defined by the inequalities

$$-\frac{1}{3}\leqslant q_1\leqslant\frac{1}{6},\quad \sqrt{q_2^2+q_3^2}\leqslant q_1+\frac{1}{3}.$$

The origin of the q space corresponds to the isotropic state ($\mathbf{Q}=\mathbf{0}$). It is crucial to our analysis to identify in the q space all uniaxial states. We find that they can be of one of two types, either uniaxial with director along the x axis (normal to the boundary surfaces) or uniaxial with director in the y-z plane (in the plane of the boundary surfaces). The line

$$q_2=q_3=0 \tag{5}$$

represents uniaxial states of the former type, since along it $\lambda_2=\lambda_3$, while the conical surface

$$9q_1^2=q_2^2+q_3^2 \tag{6}$$

corresponds to uniaxial states of the latter type: more precisely, $\lambda_1=\lambda_3$ when $q_1<0$, and $\lambda_1=\lambda_2$ when $q_1>0$. This geometric representation of the uniaxial states was first introduced in Ref. [11] and then used in Refs. [12,13] to classify both surface and bulk defects arising in nematic liquid crystals. As we shall see, this representation plays a key role in detecting order reconstruction.

The boundary conditions (2) and (3), in the q representation, take the form

$$q_1(-d)=\frac{s_b}{6},\quad q_1(d)=\frac{s_b}{6}, \tag{7a}$$

$$q_2(-d)=\frac{s_b}{2},\quad q_2(d)=\frac{s_b}{2}\cos 2\phi_0, \tag{7b}$$

$$q_3(-d)=0,\quad q_3(d)=\frac{s_b}{2}\sin 2\phi_0. \tag{7c}$$

Both points $q(-d)$ and $q(d)$ belong to the uniaxial cone defined by Eq. (6), for all values of s_b.

III. FREE ENERGY

In this section, we build the free-energy functional that is stationary in all equilibrium configurations within the twist cell $\mathcal{B}$ described above.

A. Bulk potential

In the classical Landau–de Gennes theory (see Ch. 2 of Ref. [8]), the bulk potential that describes a homogeneous phase is given by

$$f_b:=\frac{A}{2}\,\mathrm{tr}\,\mathbf{Q}^2-\frac{B}{3}\,\mathrm{tr}\,\mathbf{Q}^3+\frac{C}{4}(\mathrm{tr}\,\mathbf{Q}^2)^2. \tag{8}$$

Here B and C are positive constitutive parameters, while A depends on the temperature T in the form $A=a(T-T^*)$, with a a positive constant and T^* the nematic *supercooling* temperature. In the q representation, the invariants of $\mathbf{Q}$ read as

$$\mathrm{tr}\,\mathbf{Q}^2=2(3q_1^2+q_2^2+q_3^2),\quad \mathrm{tr}\,\mathbf{Q}^3=-6q_1(q_1^2-q_2^2-q_3^2), \tag{9}$$

and the bulk potential (8) takes the form

$$f_b=A(3q_1^2+q_2^2+q_3^2)+2Bq_1(q_1^2-q_2^2-q_3^2)+C(3q_1^2+q_2^2+q_3^2)^2. \tag{10}$$

In a homogeneous phase, the eigenvectors of $\mathbf{Q}$, though arbitrary, are fixed in space. Letting them coincide with the frame $\{\boldsymbol{e}_x,\boldsymbol{e}_y,\boldsymbol{e}_z\}$, we can adopt for $\mathbf{Q}$ the q representation with $q_3=0$, so that q_2 itself represents a measure of biaxiality. If for any order tensor $\mathbf{Q}$, either uniaxial or biaxial, we formally define the scalar order parameter s through the equation

$$\mathrm{tr}\,\mathbf{Q}^2=\frac{2}{3}s^2=2(3q_1^2+q_2^2),$$

then for positive s we can express q_1 as

$$q_1=-\frac{1}{3}\sqrt{s^2-3q_2^2},$$

and Eq. (10) for f_b (with $q_3=0$) can be written as

$$f_b=\frac{1}{3}\left[As^2-\frac{2}{9}B\sqrt{s^2-3q_2^2}(s^2-12q_2^2)+\frac{1}{3}Cs^4\right]. \tag{11}$$

For any given $s>0$, this function is minimized by $q_2=0$, and we conclude that in the absence of any externally imposed frustration, the only stable equilibrium states would be uniaxial. In this limit, Eq. (11) becomes

$$f_0(s)=\frac{1}{3}As^2-\frac{2}{27}Bs^3+\frac{1}{9}Cs^4. \tag{12}$$

The function f_0 above possesses three stationary points: one is attained at $s=0$, and the other two are attained at

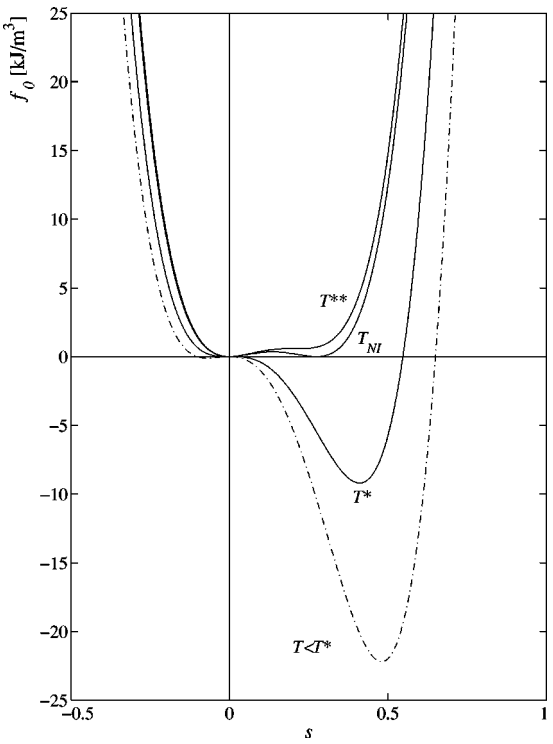

FIG. 2. The uniaxial bulk potential function f_0 against the scalar order parameter s at the critical temperatures $T=T^{**}$ (superheating), T_{NI} (nematic-isotropic transition), and T^* (supercooling), and at a temperature $T<T^*$ (dashed line). The parameters $a=0.20\times10^6$ J/Km^3, $B=7.2\times10^6$ J/m^3, and $C=8.8\times10^6$ J/m^3 correspond to those measured for 5CB(4-cyano-4′*n*-pentylbiphenyl) in Ref. [14].

$$s_\pm := \frac{B \pm \sqrt{B^2 - 24AC}}{4C}. \tag{13}$$

When $A=A_*:=B^2/24C$, s_- and s_+ coalesce in a single value $s_*:=B/4C$, where the graph of f_0 against s has an inflection point. The temperature $T^{**}:=T^*+B^2/24aC$ at which this happens is called the *superheating* temperature. At the temperature $T_{NI}:=T^*+B^2/27aC<T^{**}$, the function f_0 in Eq. (12) has two distinct minimizers, with the same minimum, namely, $s=0$ and $s=s_0:=4s_*/3$ (see Fig. 2). This is the temperature where the transition from nematic to isotropic takes place. Finally, at the supercooling temperature T^*, the graph of f_0 develops an inflection point at $s=0$: below this temperature, the isotropic state fails to be metastable. We have found it convenient to introduce the *reduced* temperature θ defined as

$$\theta := \frac{A}{A_*} = \frac{T-T^*}{T^{**}-T^*}. \tag{14}$$

Thus θ is the temperature below the supercooling point measured in units of the temperature range where both nematic and isotropic phases coexist; for low-molecular-weight liquid crystals, this range is typically $1°-2°$ wide, depending on the purity of the sample.

Other authors [7,15,16] instead prefer to define $\tau:=(T-T^*)/(T_{NI}-T^*)$ as reduced temperature. It is easily seen that $\theta=8\tau/9$. In our development below, we shall assume that $\theta\leqslant 1$, so that an ordered phase exists in the bulk. By Eq. (14), we can recast Eq. (13) as

$$s_\pm := s_*(1 \pm \sqrt{1-\theta}).$$

The equilibrium value of s, which would be preferred in the undistorted bulk for $\theta<\frac{8}{9}$, is $s_b=s_+$, and this is the value we shall use for s_b in both boundary conditions (2) and (3).

B. Elastic energy and equilibrium equations

The free energy consists of two distinct contributions: the bulk potential f_b, which inhibits departures of $\mathbf{Q}$ from the preferred uniaxial state (and its preferred degree of orientational order), and the elastic energy f_e, which penalizes distortions in space of the eigenframe of $\mathbf{Q}$ and spatial variations in the degree of order. Thus, the free-energy functional $\mathcal{F}$ takes the general form

$$\mathcal{F}[\mathbf{Q}] := \int_{\mathcal{B}} (f_e + f_b)\, dV, \tag{15}$$

where dV is volume measure. Here we adopt for f_e the following one-constant approximation:

$$f_e := \frac{L}{2}|\boldsymbol{\nabla}\mathbf{Q}|^2,$$

where $L>0$ is an elastic constant assumed independent of the temperature T.

When $\mathbf{Q}$ is prescribed on $\partial\mathcal{B}$, the equilibrium equations for $\mathcal{F}$ can be obtained as follows. We perturb $\mathbf{Q}$ by setting

$$\mathbf{Q}_\varepsilon := \mathbf{Q} + \varepsilon\mathbf{U},$$

where $\mathbf{U}$ is a symmetric, traceless tensor field subject to $\mathbf{U}|_{\partial\mathcal{B}}=\mathbf{0}$. Heeding that both $\mathbf{Q}$ and $\mathbf{U}$ are symmetric, we give the first variation of $\mathcal{F}$ the following expression:

$$\begin{aligned}\delta\mathcal{F}[\mathbf{Q}](\mathbf{U}) &:= \left.\frac{\mathrm{d}\mathcal{F}[\mathbf{Q}_\varepsilon]}{\mathrm{d}\varepsilon}\right|_{\varepsilon=0} \\ &= \int_{\mathcal{B}} \{L\boldsymbol{\nabla}\mathbf{Q}\cdot\boldsymbol{\nabla}\mathbf{U} + [A\mathbf{Q} - B\mathbf{Q}^2 \\ &\quad + C(\mathrm{tr}\,\mathbf{Q}^2)\mathbf{Q} + \lambda\mathbf{I}]\cdot\mathbf{U}\}\, dV,\end{aligned}$$

where λ is an unknown Lagrange multiplier field. Integrating by parts in the preceding integral and using the boundary conditions on $\mathbf{U}$, we arrive at

$$\begin{aligned}\delta\mathcal{F}[\mathbf{Q}](\mathbf{U}) &= \int_{\mathcal{B}} [-L\Delta\mathbf{Q} + A\mathbf{Q} - B\mathbf{Q}^2 \\ &\quad + C(\mathrm{tr}\,\mathbf{Q}^2)\mathbf{Q} + \lambda\mathbf{I}]\cdot\mathbf{U}\, dV,\end{aligned}$$

where $\Delta\mathbf{Q}$ is the Laplacian of $\mathbf{Q}$. From the arbitrariness of $\mathbf{U}$, we conclude that

$$-L\Delta\mathbf{Q}+A\mathbf{Q}-B\mathbf{Q}^2+C(\mathrm{tr}\,\mathbf{Q}^2)\mathbf{Q}+\frac{B}{3}(\mathrm{tr}\,\mathbf{Q}^2)\mathbf{I}=\mathbf{0}, \tag{16}$$

where λ has been determined by requiring the solutions to be traceless.

In the special case of interest to us, $\mathbf{Q}$ depends on the single space variable x, and so Eq. (16) becomes

$$-L\mathbf{Q}''+A\mathbf{Q}-B\mathbf{Q}^2+C(\mathrm{tr}\,\mathbf{Q}^2)\mathbf{Q}+\frac{B}{3}(\mathrm{tr}\,\mathbf{Q}^2)\mathbf{I}=\mathbf{0}, \tag{17}$$

where a prime denotes differentiation with respect to x. By taking the inner product of both sides of Eq. (17) with $\mathbf{Q}'$, we obtain the first integral

$$-\frac{L}{2}|\mathbf{Q}'|^2+\frac{A}{2}\,\mathrm{tr}\,\mathbf{Q}^2-\frac{B}{3}\,\mathrm{tr}\,\mathbf{Q}^3+\frac{C}{4}(\mathrm{tr}\,\mathbf{Q}^2)^2=-H, \tag{18}$$

where H is an integration constant. This equation, which has the appearance of a conservation law, has a further consequence, which we record here for later use. Since $(\mathrm{tr}\mathbf{Q}^2)''=2(|\mathbf{Q}'|^2+\mathbf{Q}\cdot\mathbf{Q}'')$, by Eqs. (17) and (18), we arrive at

$$\frac{L}{2}(\mathrm{tr}\,\mathbf{Q}^2)''=2H+2A\mathrm{tr}\,\mathbf{Q}^2-\frac{5}{3}B\,\mathrm{tr}\,\mathbf{Q}^3+\frac{3}{2}C(\mathrm{tr}\,\mathbf{Q}^2)^2, \tag{19}$$

an equilibrium equation for $\mathrm{tr}\,\mathbf{Q}^2$ in which the invariant $\mathrm{tr}\,\mathbf{Q}^3$ also appears.

C. Nondimensional form

To prepare the way for the numerical computations to be performed in the following section, it is convenient to write in nondimensional form both the functional $\mathcal{F}$ and the equilibrium equations associated with it. To this end, we first introduce the *biaxial* coherence length ξ_b as

$$\xi_b:=\sqrt{\frac{L}{Bs_+}}=\left[\frac{4LC}{B^2(\sqrt{1-\theta}+1)}\right]^{1/2}.$$

This length clearly depends on the temperature. Apart from some nominal differences, this length is precisely the same as the one introduced in Ref. [16] (see, in particular, the Appendix there for a rationale behind this definition). Moreover, we set

$$\overline{\mathbf{Q}}:=\frac{1}{s_*}\mathbf{Q},\quad \overline{s_b}:=\frac{s_b}{s_*},\quad \overline{x}:=\frac{x}{d},$$

where s_* is the bulk equilibrium value of s at the superheating temperature T^{**} (as defined in Sec. III A), and we express L in terms of ξ_b. We thus obtain

$$\mathcal{F}[\mathbf{Q}]=F_0\int_{-1}^{1}\left[\left(\frac{\xi_b}{d}\right)^2(\sqrt{1-\theta}+1)\left(\frac{d\overline{\mathbf{Q}}}{d\overline{x}}\right)^2+\frac{\theta}{6}\,\mathrm{tr}\,\overline{\mathbf{Q}}^2-\frac{2}{3}\,\mathrm{tr}\,\overline{\mathbf{Q}}^3+\frac{1}{8}(\mathrm{tr}\,\overline{\mathbf{Q}}^2)^2\right]d\overline{x},$$

where $F_0:=3A_*B^2d/4C^2$. To avoid clutter, we drop all bars, thus arriving at the following nondimensional form of the free-energy functional:

$$F[\mathbf{Q}]:=\frac{\mathcal{F}[\mathbf{Q}]}{F_0}=\int_{-1}^{1}\left[\frac{\xi_b^2}{d^2}(\sqrt{1-\theta}+1)|\mathbf{Q}'|^2+\frac{\theta}{6}\,\mathrm{tr}\,\mathbf{Q}^2-\frac{2}{3}\,\mathrm{tr}\,\mathbf{Q}^3+\frac{1}{8}(\mathrm{tr}\,\mathbf{Q}^2)^2\right]dx. \tag{20}$$

In the q representation for the scaled order tensor, the dimensionless free energy takes the form

$$F[q]=2\int_{-1}^{1}\left\{\frac{\xi_b^2}{d^2}(\sqrt{1-\theta}+1)[3(q_1')^2+(q_2')^2+(q_3')^2]+\frac{\theta}{6}(3q_1^2+q_2^2+q_3^2)+2q_1(q_1^2-q_2^2-q_3^2)+\frac{1}{4}(3q_1^2+q_2^2+q_3^2)^2\right\}dx, \tag{21}$$

and the equilibrium equations for F read

$$\frac{\xi_b^2}{d^2}(\sqrt{1-\theta}+1)q_1''=\frac{\theta}{6}q_1-\frac{1}{3}(q_2^2+q_3^2-3q_1^2)+\frac{1}{2}(3q_1^2+q_2^2+q_3^2)q_1, \tag{22a}$$

$$\frac{\xi_b^2}{d^2}(\sqrt{1-\theta}+1)q_2''=\frac{\theta}{6}q_2-2q_1q_2+\frac{1}{2}(3q_1^2+q_2^2+q_3^2)q_2, \tag{22b}$$

$$\frac{\xi_b^2}{d^2}(\sqrt{1-\theta}+1)q_3''=\frac{\theta}{6}q_3-2q_1q_3+\frac{1}{2}(3q_1^2+q_2^2+q_3^2)q_3. \tag{22c}$$

This coupled system of ordinary differential equations is thus the nondimensional form of Eq. (17) and the cornerstone of the numerical modeling to follow.

A special solution of this system deserves attention. If $\theta=-8$, then $s_b=4$ and $q_1(\pm d)=\frac{2}{3}$. Indeed, for this special choice of θ, $q_1(x)\equiv\frac{2}{3}$ solves Eq. (22a), as can be seen by direct inspection. So, at least in this particular case, the eigenvalue of $\mathbf{Q}$ along the direction $\boldsymbol{e}_x$ remains constant across the cell. This will often be employed below as a comparison case.

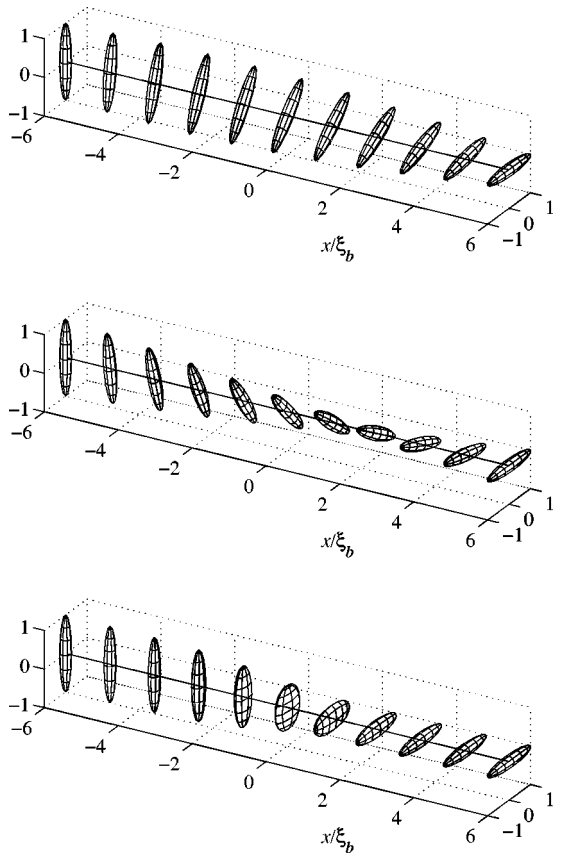

FIG. 3. Order-tensor ellipsoids against position across the cell, in units of the biaxial coherence length ξ_b, for three basic solutions: opposite twists (top and middle) and eigenvalue exchange (bottom). Ellipsoids are oriented along the eigenframe of the order tensor **Q** at each point; their semiaxes are the eigenvalues of **Q** appropriately augmented and scaled to the largest eigenvalue at the boundary. Parameters: twist angle $\phi_0=\pi/2$, reduced temperature $\theta=-8$, and dimensionless cell half-width $d/\xi_b=6$.

IV. NUMERICAL MODELING AND EQUILIBRIUM CONFIGURATIONS

For each fixed value of the twist angle ϕ_0, reduced temperature θ, and dimensionless half-width of the cell, d/ξ_b, we determine the solutions for the scalar fields q_1, q_2, q_3 to the equilibrium equations (22) subject to the boundary conditions (7). In general, Eqs. (22) have more than one solution. First, the same boundary conditions could be obeyed by two twist solutions, corresponding to opposite rotations of the eigenframe of **Q** across the cell. In addition, a third type of solution can be found in which the liquid crystal is uniaxial along the direction imposed by the boundary conditions on the plates, but, in the neighborhood of the center of the cell, it tends to become uniaxial in the direction normal to the boundaries, namely, $\boldsymbol{e}_x$, with a negative order parameter. Illustrations of these three types of solutions are given in Fig. 3, where both the eigenvalues and the eigenvectors of **Q** are pictorially represented through ellipsoids.

Very good software tools are available for the numerical modeling of problems such as the one at hand. For this investigation, we have relied upon MATLAB [24], AUTO 97 [17], and AUTO 2000 [25]. MATLAB is a commercial scientific computing and visualization environment. With its high-level language syntax, wealth of mathematical library software, and integrated graphics, it is an excellent tool for the numerical modeling of a wide array of problems. We have used primarily the MATLAB graphics, as well as a code from its ODE suite, bvp4c, for the solution of general nonlinear systems of ordinary differential equations.

The MATLAB BVP solver is not equipped for numerical bifurcation analysis, and for that we have relied upon the AUTO package. This venerable code has been a mainstay of the numerical bifurcation and dynamical systems communities for over two decades. For ODE boundary value problems, the package has the capabilities to perform parameter continuation, detection of bifurcation points, and stable numerical calculation of limit points. It is also capable of monitoring auxiliary integral functionals, such as the free energy, and of generating a two-parameter locus of fold points. We have used all of these features to obtain the results we discuss below.

V. BIFURCATION UNFOLDING

As anticipated in Sec. IV, solutions to Eqs. (22) are found in three different classes. The members of two of them resemble a regular twist, whilst the members of the third class are *exchange* solutions, here called the χ solutions for short, which mimic the solution of Palffy-Muhoray *et al.* [2] characterized by a local biaxial transition. For every value of $\phi_0 \in]0,\pi/2[$, the total twist of the director across the cell for the two twist solutions is either ϕ_0 or $\pi-\phi_0$: hereafter, the former solutions will be referred to as the τ_- solutions, and the latter as the τ_+ solutions. For $\phi_0=0$, coherently with the normalization adopted here, the τ_+ solution is a π twist and the corresponding τ_- solution is the uniform state of the director. For $\phi_0=\pi/2$, τ_+ and τ_- solutions are symmetric to one another, but there is no intrinsic way to tell which is which because they both exhibit the same total twist. However, such an ambiguity plays no role in our development. Our calculations show that a τ_- solution always minimizes the free-energy functional $\mathcal{F}$ in Eq. (15), whereas all τ_+ solutions are at most metastable, and all χ solutions are always locally unstable. A clear indication of this instability is that an initial guess must be appropriately built to compute a χ solution through a numerical parameter continuation.

A. Polar plots

Recalling our discussion in Sec. III A, we can represent solutions of Eqs. (22) by a curve $\mathcal{C}$ in the q space. $\mathcal{C}$ intersects the loci (5) and (6) wherever it attains a uniaxial state. Equation (7a) shows that q_1 has one and the same value on the plates bounding the cell. Moreover, numerical solutions of Eqs. (22) reveal that q_1 is nearly constant across the cell. As discussed in Sec. III A, q_1 is indeed constant, when $\theta=-8$. This suggests one to study the projection of $\mathcal{C}$ onto the (q_2,q_3) plane, for all solutions of Eqs. (22). We shall refer to such a projection as to the *polar plot* of the solution.

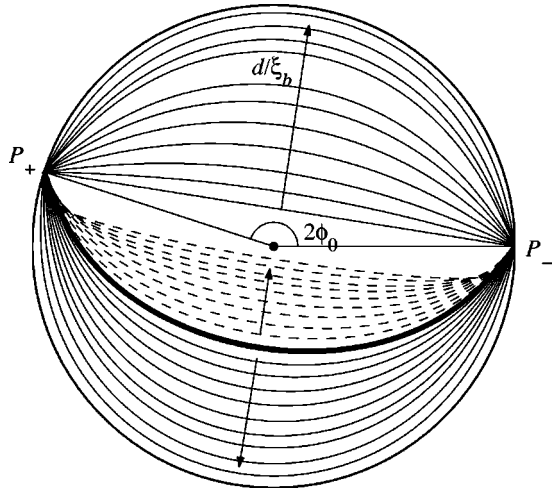

FIG. 4. Polar plot of q_2, q_3 components of order-tensor equilibrium solutions. Parameters: twist angle $\phi_0=0.45\pi$, reduced temperature $\theta=-8$, and several values of dimensionless cell half-width $d/\xi_b \leqslant 8$. Upper curves correspond to less twisted solutions τ_-, approaching uniaxial states on the circumference as d/ξ_b increases. Lower solid curves correspond to more twisted solutions τ_+, while lower dashed curves are eigenvalue-exchange solutions χ. These merge in the heavy line as d/ξ_b decreases to the critical value $d/\xi_b \simeq 3.33$. The arrows indicate in which sense d/ξ_b is increased for the different classes of solutions. The center of the circumference corresponds to the whole family of uniaxial states with negative order parameter described by Eq. (5)

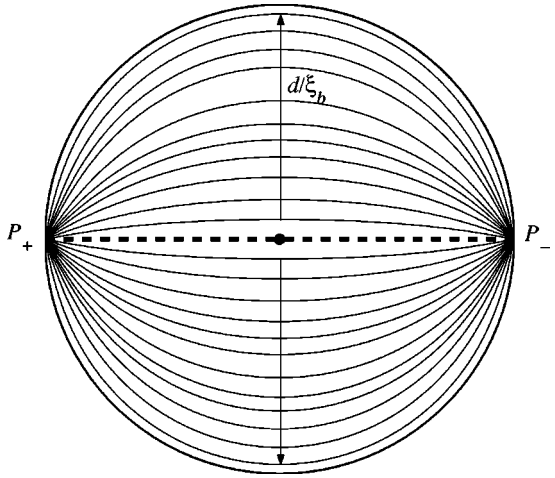

FIG. 5. Polar plot of q_2, q_3 components of order-tensor equilibrium solutions. Parameters: twist angle $\phi_0=\pi/2$, reduced temperature $\theta=-8$, and several values of dimensionless cell half-width d/ξ_b ranging between 2.475 and 8 in the sense indicated by the arrows. Exchange solutions run along the horizontal axis for all values of d/ξ_b. The remaining, symmetric curves correspond to the symmetric twisted solutions. These approach uniaxial states on the circumference as d/ξ_b increases, and they merge into the exchange solution as d/ξ_b decreases to the critical value $d/\xi_b \simeq 2.47$, below which the twisted solutions fail to exist. The solutions in real space corresponding to the largest value of d/ξ_b considered here are illustrated in Fig. 3.

As will soon be shown, polar plots are crucial to understand the patterns of orientational order for solutions in different classes. We see from Eqs. (7b)–(7c) that all polar plots must pass through two points, P_- and P_+, on the circle $q_2^2+q_3^2=s_b^2/4$, which is the (q_2,q_3) projection of the intersection between the uniaxial cone (6) and the plane $q_1=s_b/6$. We choose polar coordinates (ϱ,ϑ) in the (q_2,q_3) plane so that $P_-\equiv(s_b/2,0)$ and $P_+\equiv(s_b/2,2\phi_0)$. Thus, P_- represents the boundary condition on the lower plate, and P_+ that on the upper plate. Figure 4 shows typical polar plots for $\theta=-8$, and $\phi_0=0.45\pi$.

We see that τ_- solutions tend to become uniaxial across the whole cell, when d/ξ_b increases. Moreover, they all reside in the circular sector above the line segment joining P_- and P_+, while both τ_+ and χ solutions reside in the circular sector below this segment. Upon decreasing d/ξ_b, the single τ_+ and χ solutions approach each another until a critical value is reached (e.g., $d/\xi_b \simeq 3.33$ for $\theta=-8$), where they merge together. For lower values of d/ξ_b, only τ_- solutions exist. For a given value of d/ξ_b, the corresponding τ_- solution is the absolute energy minimizer; the equilibrium solutions with higher energy, in either class τ_+ or χ, can relax to it only by crossing the origin of the (q_2,q_3) plane: correspondingly, the curve $\mathcal{C}$ would cross the uniaxial line (5) at the point where the order reconstruction actually occurs in the cell. The line (5) thus separates the energy minimizers from all other equilibrium solutions.

A slightly different scenario occurs for the symmetric case where $\phi_0=\pi/2$. Here, τ_- and τ_+ solutions are symmetric, and so are their polar plots with respect to the line $\vartheta=0$, as shown in Fig. 5: χ solutions now exist for values of d/ξ_b down to 0 and all their polar plots coalesce into the line segment joining P_- and P_+. As the cell thickness d/ξ_b is decreased, twist solutions become more and more strained and, correspondingly, more and more biaxial near the center of the cell, until a critical value is reached ($d/\xi_b \simeq 2.47$ for $\theta=-8$), where they merge with the χ solution. Below this threshold, no twist solution exists.

Furthermore, the limiting case where $\phi_0 \to 0$ also deserves attention. Here, the τ_- solution tends to represent the uniform state across the cell, whereas the τ_+ solution tends to be a π twist. Polar plots with $\phi_0=0$ are shown in Fig. 6. A pictorial way to obtain Fig. 6 from Fig. 4 is the following. We move the point P_+ along the circumference in Fig. 4 until it coalesces with P_-. Correspondingly, the polar plots of all τ_- solutions collapse into the singleton $P\equiv P_-\equiv P_+$, while the polar plots of both τ_+ and χ solutions turn around the origin. We see from Fig. 6 that the uniaxial line (5) still exerts the same topological separation as above. As in Fig. 4, there is a critical value of the cell thickness d/ξ_b at which τ_+ and χ solutions merge together. It turns out that this threshold increases, as the intuition suggests: indeed, for $\theta=-8$, merging of solutions occurs when $d/\xi_b \simeq 7.72$. Again, upon further decreasing d/ξ_b, only τ_- solutions survive.

However, the χ solution seems somewhat artificial in this context, as the eigenvalue exchange merely accommodates an effective π rotation of the eigenframe of $\mathbf{Q}$ via a biaxial transition which occurs in a narrow region around the middle of the cell. This rotation is shown in Fig. 7: the more the

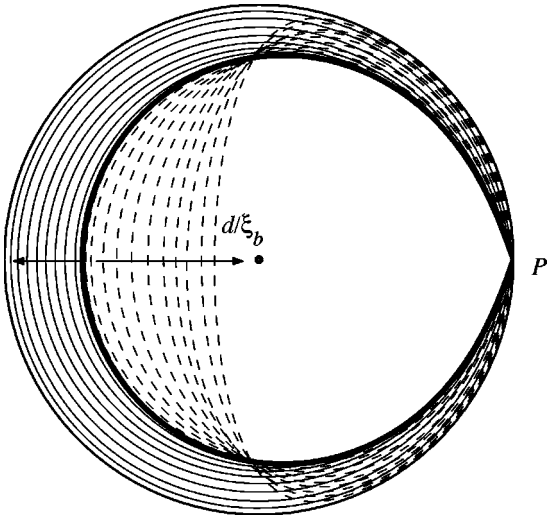

FIG. 6. Polar plot of q_2, q_3 components of order-tensor equilibrium solutions. Parameters: twist angle $\phi_0=0$, reduced temperature $\theta=-8$, and several values of dimensionless cell half-width $d/\xi_b \leqslant 20$. Solid curves correspond to π-twist solutions, approaching uniaxial states on the circumference as d/ξ_b increases. Dashed curves correspond to eigenvalue-exchange solutions. These merge in the heavy line as d/ξ_b decreases to the critical value $d/\xi_b \simeq 7.72$.

ratio d/ξ_b increases, the narrower becomes the region where the reorientation takes place. This behavior can also be read in Fig. 6 where the polar plots of the exchange solutions approach a peculiar curve in the limit case as $d/\xi_b \to \infty$: this curve moves from P along the upper-left quadrant until the point $(s_b/2,\pi/2)$ is reached; then it suddenly jumps to the opposite point $(s_b/2,3\pi/2)$ and then travels back to P along the lower-left quadrant.

B. Bifurcation diagrams

Inspection of the polar plots also suggests how to choose the parameter to capture the behavior of the solutions in a bifurcation diagram. In fact, for a fixed value of the cell thickness, along any polar plot the function $\rho(q_2,q_3) := \sqrt{q_2^2+q_3^2}$ attains its minimum in a single point. The function ρ measures the distance of a solution from the uniaxial loci (5) and (6): where $\rho=0$, the corresponding solution is uniaxial along the direction $\boldsymbol{e}_x$, orthogonal to the plates; where $\rho=s_b/2$, the solution is uniaxial along a direction parallel to the plates.

Given the role of topological separation played by the origin of the (q_2,q_3) plane, we can introduce the following dimensionless bifurcation parameter:

$$r := \pm \min \rho(q_2,q_3),$$

where the minimum is computed along a polar plot, and the sign is positive for τ_- solutions and negative for all others. Figure 8 shows some bifurcation diagrams, where the parameter r is plotted against the cell dimensionless half-width d/ξ_b, for $\theta=-8$ and three values of ϕ_0, that is, $\phi_0=0$, 0.45π, and $\pi/2$. Three families of lines correspond in Fig. 8

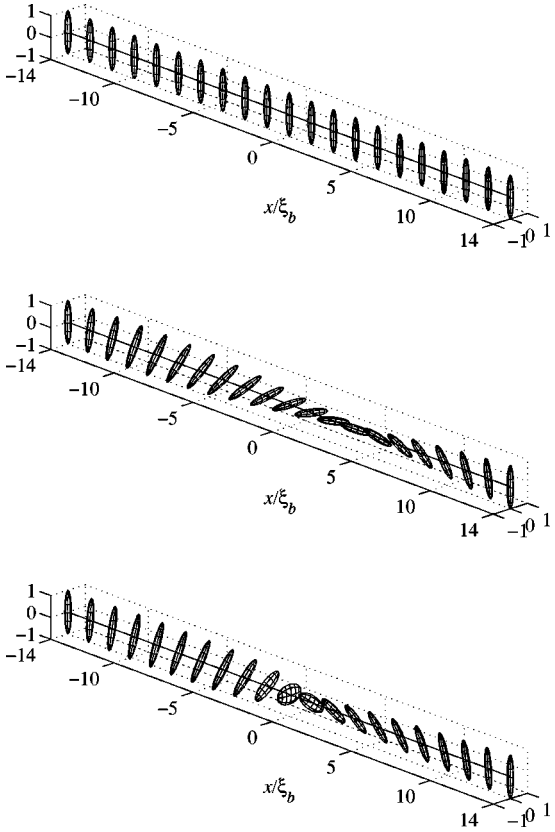

FIG. 7. Order-tensor ellipsoids against position across the cell, in units of the biaxial coherence length ξ_b, for three basic solutions: uniform uniaxial alignment (top), π twist (middle), and eigenvalue-exchange solution (bottom). Ellipsoids are oriented along the eigenframe of the order tensor $\mathbf{Q}$ at each point; their semiaxes are the eigenvalues of $\mathbf{Q}$ appropriately augmented and scaled to the largest eigenvalue at the boundary. Parameters: twist angle $\phi_0=0$, reduced temperature $\theta=-8$, and dimensionless cell half-width $d/\xi_b=14$.

to these values of ϕ_0: they are labeled (a), (b), and (c), respectively, and all have three branches. The branch of (a) at $r=s_b/2$, which equals 2 for $\theta=-8$, corresponds to the uniform state with director along $\boldsymbol{e}_x$ across the whole cell. The negative branches of (a) represent the metastable π twist and the corresponding χ solution. The positive branch of (b) exists regardless of the value of d/ξ_b, and it approaches the value $r \simeq 0.313$ when d/ξ_b goes to 0. In this limit, all τ_- solutions have a high degree of biaxiality in the center of the cell, while they become closer and closer to a pure uniaxial twist when d/ξ_b is large. The corresponding τ_+ and χ solutions are represented by the negative branches of line (b). Upon increasing ϕ_0, the turning point where these solutions merge together moves towards the r axis that is indeed reached when $\phi_0=\pi/2$, where the bifurcation diagram turns into the pitchfork (c). In the jargon of bifurcation analysis and singularity theory, we can say that the twist angle ϕ_0 provides a *universal unfolding* of the one-parameter, symmetric pitchfork (see, e.g., the review paper Ref. [18], and references therein). The dotted curve in Fig. 8 is the *spinodal curve* that separates metastable states from unstable states: it can be viewed as the locus of the turning points of the diagram, as a function of ϕ_0.

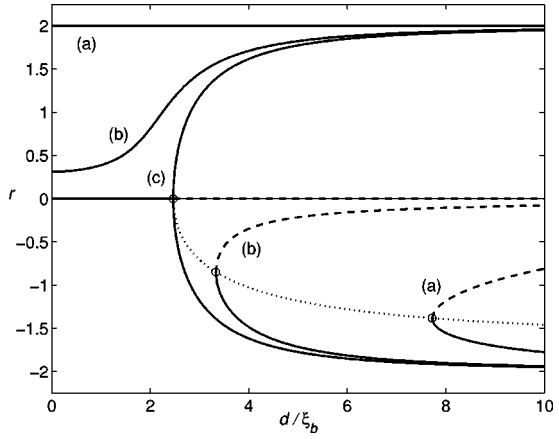

FIG. 8. Bifurcation diagram of r against the dimensionless half-width d/ξ_b of the cell, for several solution paths. Parameters: reduced temperature $\theta=-8$, total twist angles: (a) $\phi_0=0$, (b) $\phi_0=0.45\pi$, and (c) $\phi_0=\pi/2$. Curves: solid (metastable), dashed (locally unstable), and dotted (spinodal curve).

One feature of the bifurcation diagram of Fig. 8 can be explained analytically: the asymptotic behavior of τ_- solutions when $d/\xi_b \ll 1$. Regarding d/ξ_b as a perturbation parameter in Eqs. (22), and using the exact solutions of these equations for the limiting case where $d/\xi_b=0$, we can prove that r has the following parabolic behavior:

$$r=\frac{s_b}{2}\cos\phi_0\left\{1-\frac{1}{2(\sqrt{1-\theta}+1)}\left(\frac{d}{\xi_b}\right)^2 \times\left[\frac{\theta}{6}-\frac{s_b}{3}+\frac{s_b^2}{48}(3+5\cos^2\phi_0)\right]\right\}+O\left[\left(\frac{d}{\xi_b}\right)^4\right].$$

Similar computations have been performed for values of $\theta \ll -8$; in particular, we have produced polar plots and bifurcation diagrams for $\theta=-48$ and $\theta=-4899$: their features were found to be qualitatively the same as those shown here, quantitatively, the turning point approaches the r axis as θ decreases.

VI. DISCUSSION

In this section we discuss two separate questions that could be raised quite naturally at this stage. One is about boundary conditions, which here have systematically been taken as uniaxial on both plates. The other is about the validity of an approximation often used in the analysis of the biaxial structure of defects, which here has systematically been ignored.

A. Biaxial boundary conditions

The uniaxial boundary conditions imposed on the two plates of the cell are represented by Eqs. (7). We now alter these equations to accommodate a special class of biaxial boundary conditions. We leave the conditions for q_1 unchanged, while we write those for q_2 and q_3 as follows

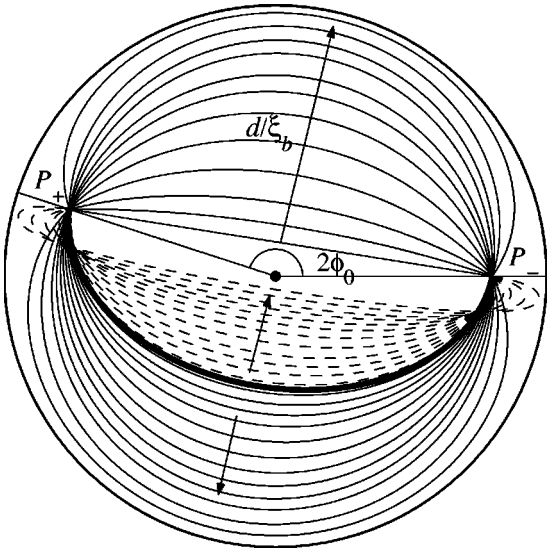

FIG. 9. Polar plot of q_2, q_3 components of order-tensor equilibrium solutions with special biaxial boundary conditions. Parameters: twist angle $\phi_0=0.45\pi$, reduced temperature $\theta=-8$, parameter of biaxiality $\varepsilon=-0.2$, and several values of dimensionless cell half-width $d/\xi_b \leqslant 8$. Upper curves correspond to less twisted solutions τ_-, approaching uniaxial states on the circumference as d/ξ_b increases. Lower solid curves correspond to more twisted solutions τ_+, while lower dashed curves are eigenvalue-exchange solutions χ. These merge in the heavy line as d/ξ_b decreases to the critical value $d/\xi_b \simeq 3.10$. The arrows indicate for the different classes of solutions in which sense d/ξ_b is increased.

$$q_2(-d)=\frac{s_b}{2}(1+\varepsilon), \quad q_2(d)=\frac{s_b}{2}(1+\varepsilon)\cos 2\phi_0, \tag{23a}$$

$$q_3(-d)=0, \quad q_3(d)=\frac{s_b}{2}(1+\varepsilon)\sin 2\phi_0. \tag{23b}$$

In the q space, these boundary points live away from the uniaxial cone (6) for every $\varepsilon\neq 0$; in particular, for $\varepsilon>0$ they are both outside this cone, while for $\varepsilon<0$ they are both inside it. The order tensor $\mathbf{Q}^-$ corresponding to $q(-d)$ can then be represented as

$$\mathbf{Q}^-=s\left(\boldsymbol{e}_z\otimes\boldsymbol{e}_z-\frac{1}{3}\mathbf{I}\right)+t(\boldsymbol{e}_x\otimes\boldsymbol{e}_x-\boldsymbol{e}_y\otimes\boldsymbol{e}_y), \tag{24}$$

where

$$s=\left(1+\frac{3}{4}\varepsilon\right)s_b \quad \text{and} \quad t=\frac{1}{4}\varepsilon s_b. \tag{25}$$

It is clear from Eqs. (25) that for $\varepsilon<0$ the molecules on the lower plate are less oriented along $\boldsymbol{e}_z$ than they are for $\varepsilon>0$: the boundary biaxiality introduced in Eq. (24) has a disordering effect in the former case and an ordering effect in the latter case. The order tensor $\mathbf{Q}^+$ corresponding to $q(d)$ has the same eigenvalues as $\mathbf{Q}^-$ and an eigenframe rotated by the angle ϕ_0 about $\boldsymbol{e}_x$.

Figure 9 shows the polar plots in the (q_2,q_3) plane of the solutions to Eqs. (22) subject to Eqs. (7a) and (23), for $\varepsilon=-0.2$ and $\phi_0=0.45\pi$. Again, all solutions can be grouped in three different classes, and their behavior apparently parallels that of the solutions for $\varepsilon=0$. In particular, the uniaxial line (5) still separates τ_- solutions from all others: it must be traversed in any relaxation process starting from the τ_+ solution when this ceases to exist.

B. Lyuksyutov constraint

In Ref. [19], Lyuksyutov proposed an approximate minimization of the functional in Eq. (15), which has been often employed to explore the fine structure of defect cores [15,20]. This method relies on the observation that whenever in Eq. (8) $B \ll \sqrt{AC}$, one can treat the tr $\mathbf{Q}^3$ term in f_b as a small perturbation and first minimize the dominant part of the bulk potential, that is,

$$f_b=\frac{A}{2}\,\mathrm{tr}\,\mathbf{Q}^2+\frac{C}{4}(\mathrm{tr}\,\mathbf{Q}^2)^2,$$

thus obtaining

$$\mathrm{tr}\,\mathbf{Q}^2=-\frac{A}{C}. \tag{26}$$

Then the modified free energy

$$\mathcal{F}^*[\mathbf{Q}]=\int_{\mathcal{B}}\left(\frac{L}{2}|\nabla\mathbf{Q}|^2-\frac{B}{3}\,\mathrm{tr}\,\mathbf{Q}^3\right)dV$$

can be minimized subject to constraint (26). This approach, though based on a rather crude approximation, makes it easier to obtain analytic results from the Euler-Lagrange equations for $\mathcal{F}^*$, as shown, for example, in Refs. [15,21]. Sometimes these approximate results have formed the basis for deeper numerical explorations of the complete Landau–de Gennes model [22,23].

The question then arises of probing the validity of constraint (26) in the problem solved here. This issue is indeed related to the growth of the degree of biaxiality within the cell. Since $\mathrm{tr}\mathbf{Q}^3=3\det\mathbf{Q}$, it follows from Eqs. (1) and (19) that on the equilibrium configurations for $\mathcal{F}$, Eq. (26) is satisfied only if $\det\mathbf{Q}$ is a specific constant. Thus, the lack of uniformity in the graph of $\det\mathbf{Q}$ somewhere within the cell is an unmistakable sign that the Lyuksyutov constraint cannot be valid there. As shown in Fig. 10, the graph of $\det\mathbf{Q}$ across the cell is quite different for a τ_- and a χ solution: it is more uniform in the center than near the plates on a τ_- solution, while it is more uniform near the plates than in the center for a χ solution. Moreover, for a χ solution the less uniform $\det\mathbf{Q}$ is, the more it approaches zero, that is, the higher is the degree of biaxiality. In other words, the Lyuksyutov constraint is violated just to allow more biaxiality in the cell.

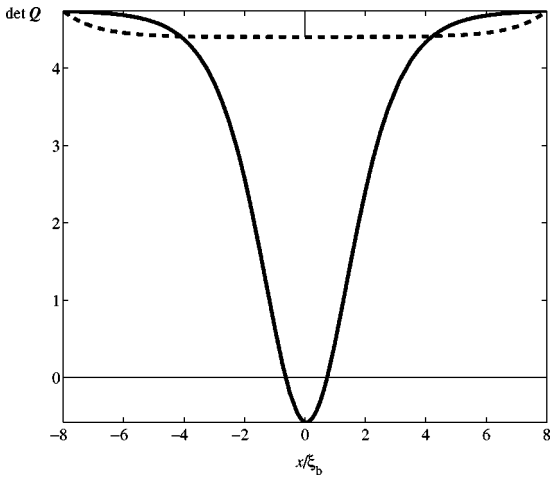

FIG. 10. The graph of $\det\mathbf{Q}$ through the cell for both a τ_- and a χ solution (dashed and solid line, respectively). Parameters: reduced temperature $\theta=-8$, twist angle $\phi_0=0.45\pi$, and dimensionless half-width of the cell $d/\xi_b=8$.

VII. SUMMARY

By use of the classical Landau–de Gennes theory we studied an equilibrium problem within a nematic cell where the plates enforce uniaxial boundary conditions with twisted directors. For a sufficiently large separation d of the plates, there are three different solutions to this equilibrium problem: two of them exhibit opposite twists of the eigenframe of the order tensor $\mathbf{Q}$, whilst the third one exhibits an exchange in the eigenvalues of $\mathbf{Q}$. The less twisted solution among these is always the energy minimizer; it exists for all values of d. On the contrary, the other two solutions exist only if d is greater than a critical value d_c, in the range of a few biaxial coherence lengths: if $d>d_c$, the exchange solution is locally unstable, while the more twisted solution is metastable. At $d=d_c$, these two branches of solutions merge together and both disappear. When this happens, the system relaxes back to the energy minimizer with a jump in the free energy: an order reconstruction then takes place on a plane in the cell where the order tensor traverses a uniaxial state with negative scalar order parameter and director orthogonal to the plates of the cell.

This scenario applies to every choice of the total twist angle across the cell but $\pi/2$: when the two boundary directors are at right angles, which is the case most studied in the literature, the two opposite twisted solutions merge continuously into the exchange solution at a critical value of the distance between the plates. Such a behavior, actually reflecting the higher symmetry in the $\pi/2$ twist, is, however, rather peculiar, as it is *unfolded* by any perturbation in the alignment of the boundary directors. All transitions studied in this paper occur when the distance between the plates is reduced down to a few biaxial coherence lenghts. While these distances are indeed very small, the outcomes of our study are in principle applicable to confinements induced by some external field.

ACKNOWLEDGMENTS

The authors are grateful to Georges Durand for helpful discussions. The work of E.C.G. was supported by the National Science Foundation under Grant No. DMS-0107761.

[1] N. Schopohl and T.J. Sluckin, Phys. Rev. Lett. **59**, 2582 (1987).
[2] P. Palffy-Muhoray, E.C. Gartland, and J.R. Kelly, Liq. Cryst. **16**, 713 (1994).
[3] G. Barbero and R. Barberi, J. Phys. (Paris) **44**, 609 (1983).
[4] H.G. Galabova, N. Kothekar, and D.W. Allender, Liq. Cryst. **23**, 803 (1997).
[5] P. Ziherl, F. Karimi Pour Haddadan, R. Podgornik, and S. Žumer, Phys. Rev. E **61**, 5361 (2000).
[6] A. Šarlah, P. Ziherl, and S. Žumer, Mol. Cryst. Liq. Cryst. Sci. Technol. Sect. A **329**, 1025 (1999).
[7] A. Šarlah and S. Žumer, Phys. Rev. E **60**, 1821 (1999).
[8] P.G. de Gennes and J. Prost, *The Physics of Liquid Crystals* 2nd ed. (Clarendon Press, Oxford, 1993).
[9] E.G. Virga, *Variational Theories for Liquid Crystals* (Chapman and Hall, London, 1994).
[10] P. Kaiser, N. Wiese, and S. Hess, J. Non-Equilib. Thermodyn. **17**, 153 (1992).
[11] P. Biscari, G. Capriz, and E.G. Virga, Liq. Cryst. **16**, 479 (1994).
[12] P. Biscari and G.G. Peroli, Commun. Math. Phys. **186**, 381 (1997).
[13] P. Biscari, G.G. Peroli, and T.J. Sluckin, Mol. Cryst. Liq. Cryst. Sci. Technol., Sect. A **292**, 91 (1997).
[14] H.J. Coles, Mol. Cryst. Liq. Cryst. Lett. **49**, 67 (1978).
[15] S. Kralj and E.G. Virga, J. Phys. A **34**, 829 (2001).
[16] S. Kralj, E.G. Virga, and S. Žumer, Phys. Rev. E **60**, 1858 (1999).
[17] E.J. Doedel, A.R. Champneys, T.F. Fairgrieve, Y.A. Kuznetsov, B. Sandstede, and X. Wang, Concordia University, 1997, available by FTP from ftp.cs.concordia.ca in the directory pub/doedl/auto
[18] K.A. Cliffe, A. Spence, and S.J. Tavener, Acta Numerica **9**, 39 (2000).
[19] I.F. Lyuksyutov, Zh. Eksp. Teor. Fiz. **75**, 358 (1987) [Sov. Phys. JETP **48**, 178 (1978)].
[20] E. Penzenstadler and H.-R. Trebin, J. Phys. (Paris) **50**, 1027 (1989).
[21] R. Rosso and E.G. Virga, J. Phys. A **29**, 4247 (1996).
[22] E.C. Gartland, Jr. and S. Mkaddem, Phys. Rev. E **59**, 563 (1999).
[23] S. Mkaddem and E.C. Gartland, Jr., Phys. Rev. E **62**, 6694 (2000).
[24] MATLAB is a registered trademark of The MathWorks, Inc. http://www.mathworks.com
[25] See http://sourceforge.net/projects/auto2000